Monthly Notices
of the
ROYAL ASTRONOMICAL SOCIETY

MNRAS **502,** 2043–2048 (2021)
Advance Access publication 2021 January 22

doi:10.1093/mnras/stab169

Characteristics of source locations and solar cycle distribution of the strong solar proton events (≥1000 pfu) from 1976 to 2018

Gui-Ming Le [1,3]★ Ming-Xian Zhao,[1]★ Qi-Li,[4] Gui-Ang Liu,[3] Tian Mao[1] and Ping-Guo Xu[2]

[1]*Key Laboratory of Space Weather, National Center for Space Weather, China Meteorological Administration, Beijing 100081, P. R. China*
[2]*School of Physics Science and Technology, Lingnan Normal University, Zhanjiang 524048, P. R. China*
[3]*Institute of Geophysics, China Earthquake Administration, Beijing 100081, P. R. China*
[4]*Beijing Engineering Research Center of Smart Mechanical Innovation Design Service, Beijing 100020, P. R. China*

Accepted 2021 January 18. Received 2021 January 18; in original form 2020 October 14

ABSTRACT

We studied the source locations and solar cycle distribution of strong solar proton events (SPEs, ≥1000 pfu) measured at the Earth from 1976 to 2018. There were 43 strong SPEs during this period. 27.9 per cent of the strong SPEs were ground level enhancement (GLE) events. We detect more strong SPEs coming from the Western hemisphere. The strong SPEs were distributed in the region of [E90–W90], extreme SPEs (≥10 000 pfu) appeared within the longitudinal area from E30 to W75, while the SPEs with peak fluxes ≥20 000 pfu concentrated in the range from E30 to W30 and were always accompanied by super geomagnetic storms (Dst ≤−250 nT). The Northern and Southern hemispheres of the Sun have 23 and 20 strong SPEs, respectively. The ranges S0–S19 and N0–N19 have 13 and 11 strong SPEs, respectively. S20–S45 and N20–N45 have 7 and 12 strong SPEs, respectively, indicating that the N-S asymmetry of strong SPEs mainly occurred in the areas with a latitude greater than 20° of the two hemispheres of the Sun. The statistical results showed that 48.8 per cent, 51.2 per cent, and 76.7 per cent of the strong SPEs appeared during the rising phase, declining phase, and in the period from two years before to the three years after the solar maximum, respectively. The number of strong SPEs during a solar cycle has a poor correlation with the solar cycle size.

Key words: Sun: particle emission – solar–terrestrial relations – sunspots.

1 INTRODUCTION

Solar proton event (SPE) is defined as an event with a peak flux greater than 10 pfu (1 particle $cm^{-2} \cdot sr^{-1} s^{-1}$) that lasts for at least 15 min for $E > 10$ MeV protons. Many SPEs have been detected by the *Geostationary Operational Environmental Satellites*. Different solar cycles have different numbers of SPEs. Shea & Smart (1990, 2002, 2007) found that except an increase in SPE occurrence with increasing solar cycle, there was no definite pattern could be recognized between the occurrence of SPEs and the solar cycle, and more SPEs occurred around solar maximum than during the other part of the solar cycle. Strong SPEs may lead to anomalies recorded by satellites in some orbits (Iucci et al. 2005). Le et al. (2014) studied the solar cycle distribution of strong SPEs from 1976 to 2006 by using old smoothed monthly mean sunspot numbers (SMMSNs). A new series of SMMSNs were reconstructed and launched in 2015 July (Clette et al. 2014, 2015, 2016; Clette & Lefèvre 2016). Starting 2015 July 1, the unrevised SMMSNs were replaced by the revised SMMSNs. The largest values of revised SMMSNs are larger than those of unrevised SMMSNs, and the time of the largest SMMSNs changed for some solar cycles compared with unrevised SMMSNs. Is the pattern of solar cycle distribution of strong SPEs in the new series of sunspot numbers different from that in the old series of sunspot numbers? To answer this question, we investigate the solar cycle distribution of strong SPEs from 1976 to 2018 by suing revised SMMSNs and compare our results with the results in the article by Le et al. (2014).

For the SPEs that occurred from 1954 to 2007, about 16 per cent of the SPEs in each solar cycle were GLE events (Shea & Smart 2001), which is a severe space weather phenomena (Shea & Smart 2012). The ratio of GLE events to strong SPEs in the period between 1976 and 2018 will be calculated. The intensity of a SPE is a function of the observation location relative to the concurrent solar activities (Shea & Smart 1996). The latitudinal and longitudinal distribution of strong SPEs from 1976 to 2018 are investigated in the present study. The SPE with peak flux ≥10000 pfu is defined as extreme SPE in this study. The solar and interplanetary phenomena, and geoeffectiveness associated with the extreme SPEs (≥10000 pfu) will also be studied. These are the motivations of the present study. Data analysis is presented in Section 2. Section 3 is discussion. Summary is given in Section 4.

2 DATA ANALYSIS

2.1 Data source

The strong SPEs during 1976–2018 were obtained from NASA from the website at https://umbra.nascom.nasa.gov/SEP/ and listed in Table A1 of Appendix A. The revised sunspot numbers were obtained

★ E-mail: legm@cma.cn (G-ML); zhaox@cma.gov.cn (M-XZ)

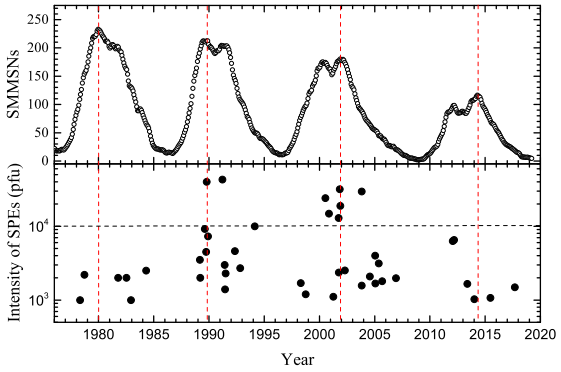

Figure 1. Strong SPEs during 1976–2018. The horizontal axis indicates time, the vertical axes in the upper and lower panels are the SMMSNs and the intensities of strong SPEs, respectively. Each red vertical dashed line marks the solar maximum of the corresponding solar cycle.

from the World Data Center SILSO, Royal Observatory of Belgium in Brussels from the website at http://sidc.oma.be/silso/datafiles. The onset time of Type II radio bursts associated with each extreme SPE, can be available from the website at ftp://ftp.ngdc.noaa.gov/STP/SOLAR_DATA/SGD_PDFversion/. The projected speed of the coronal mass ejection (CME) associated with each strong SPE was obtained from the website of coronal mass ejection (CME) catalogue at https://cdaw.gsfc.nasa.gov/CME_list/index.html. When the shock driven by the associated CME reaches the Earth's magnetosphere, it will cause a sudden storm commencement (SSC). The time of SSC is available from the Geomagnetic Reports, which are compiled by Institute of Geophysics, China Earthquake Administration.

2.2 Solar cycle distribution of strong SPEs

According to the strong SPEs listed in Table A1 of Appendix A and SMMSNs, solar cycle distribution of strong SPEs during 1976–2018 is shown in Fig. 1. To describe the characters of solar cycle distribution of strong SPEs, we use N_a, N_d, and N_{23} to indicate the numbers of the strong SPEs that appeared in the rising phase, declining phase, and in the period from two years before to the three years after the solar maximum, respectively. N_{GLE} and N_t are the numbers of GLE events and strong SPEs in a solar cycle, respectively. The largest SMMSNs is the solar cycle size (SCS). The derived N_a, N_d, N_{23}, N_{GLE}, and N_t for each solar cycle were listed in Table 1. As shown in Table 1, the larger the SCS, the lower value of N_a/N_t. We use N_{sa}, N_{sd}, N_{s23}, N_{st}, and N_{sGLE} to indicate the sum of N_a, N_d, N_{23}, N_t, and N_{GLE} during solar cycles 21–24. The derived N_{sa}/N_{st}, N_{sd}/N_{st}, N_{s23}/N_{st}, and N_{sGLE}/N_{st} are 48.8 per cent, 51.2 per cent, 76.7 per cent, and 27.9 per cent, respectively.

According to N_t and SCS, the correlation coefficient (CC) between N_t and SCS has been derived and shown in Fig. 2. We can see from

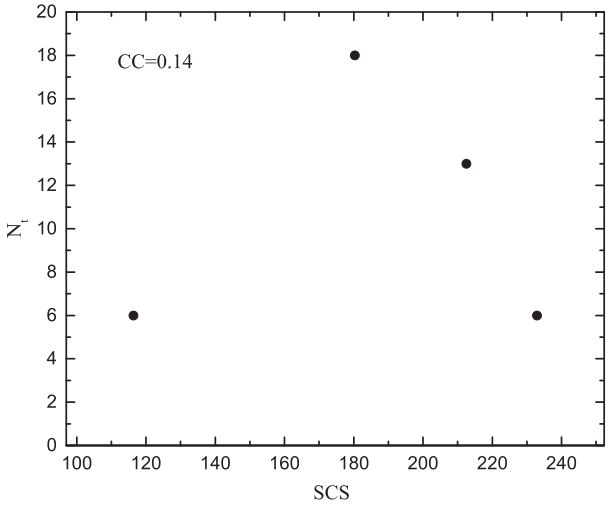

Figure 2. The correlation between N_t and SCS.

Fig. 2 that N_t has a poor correlation with SCS.

2.3 Latitudinal distribution of the strong SPEs

The latitudinal distribution of strong SPEs is shown in the left of Fig. 3. The Northern and Southern hemispheres of the Sun has 20 and 23 strong SPEs, respectively. The numbers of strong SPEs within each 10° in the two hemispheres of the Sun are listed in Table 2 and shown in the right of Fig. 3. As shown in Table 2, the number of strong SPEs within N0–N9 is the same as that within S0–S9. The difference between the number of strong SPEs within N10–N19 and that within S10–S19 is only 2. N20–N29 has one more strong SPE than S20–S29. N30–N39 has five strong SPEs, while S30–S39 has no strong SPEs.

2.4 Longitudinal distribution of the strong SPEs

The longitudinal distribution of the strong SPEs is shown in Fig. 4. Eastern and Western hemispheres of the Sun have 17 and 26 strong SPEs, respectively, indicating that more strong SPEs came from the Western hemisphere. This coincides with the concept that changed particles usually propagate along interplanetary magnetic field line, despite charged particles having perpendicular diffusion (Zhang & Zhao 2017). The strong SPEs were distributed in the range of [E90–W90]. Extreme SPEs appeared within the longitudinal area from E30 to W75, while the strong SPEs with peak intensity ≥20 000 pfu were distributed in the region from E30 to W30.

To understand the property of the longitudinal distribution of the extreme SPEs, we analyse the solar–terrestrial process for each extreme SPE. The disturbances from the Sun to the Earth, and geoeffectiveness associated with the extreme SPEs were investigated

Table 1. The number of strong SPEs appeared in different periods of solar cycles.

SC	SCS	N_a	N_d	N_{23}	N_t	N_{GLE}	N_a/N_t (per cent)	N_d/N_t (per cent)	N_{23}/N_t (per cent)	N_{GLE}/N_t (per cent)
21	232.9	2	4	5	6	2	33.3	66.7	83.3	33.3
22	212.5	6	7	12	13	3	46.2	53.8	92.3	23.1
23	180.3	9	9	11	18	6	50	50.0	61.1	33.3
24	116.4	4	2	5	6	1	66.7	33.3	83.3	16.7
Statistical average		N_{sa}	N_{sd}	N_{s23}	N_{st}	N_{sGLE}	N_{sa}/N_{st} (per cent)	N_{sd}/N_{st} (per cent)	N_{s23}/N_{st} (per cent)	N_{sGLE}/N_{st} (per cent)
		21	22	33	43	12	48.8	51.2	76.7	27.9

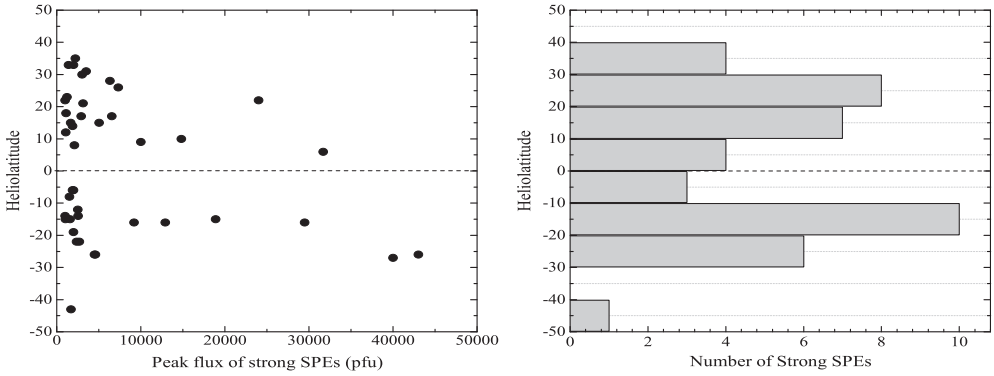

Figure 3. The left- and right-hand figures are the latitudinal distribution and N-S asymmetry of the strong SPEs, respectively.

Table 2. Latitudinal distribution of the strong SPEs during 1976–2018.

Northern hemisphere		Southern hemisphere	
Latitudinal area	Number of strong SPEs	Latitudinal area	Number of strong SPEs
N0–N9	3	S0–S9	3
N10–N19	8	S10–S19	10
N20–N29	7	S20–S29	6
N30–N39	5	S30–S39	0
N40–N49	0	S40–S49	1

and listed in Table 3. Columns 1 through out 14 are date, NOAA number of the AR, source location of the AR, the projected speed of the corresponding CME, flare intensity (FI), flare time, and the onset time of type-II radio burst. The time difference between the onset time of type-II radio burst and the SSC, and the averaged shock speed propagating from the Sun to the Earth, peak intensity of strong SPEs, the moment of SSC, Dst index, and the type of intensity–time profile (ITP) of the extreme SPE. There are two kinds of ITPs for extreme SPEs shown in Fig. 5. The flux of $E > 10$ MeV protons increased continuously until the CME-driven shock reached the magnetosphere shown in the left-hand side of Fig. 5. This kind of ITP for $E > 10$ MeV protons is defined as type P in the present study. The flux of $E > 10$ MeV protons did not increase in a sustained manner from the onset time of the SPE to the moment when the CME-driven shock reached the magnetosphere indicated by the vertical dashed line shown in the right-hand side of Fig. 5. This kind of ITP for $E > 10$ MeV protons is defined as type O in the present study.

3 DISCUSSION

(i) Unrevised SMMSNs in solar cycle 22 reached its largest value in 1989 July, and N_a/N_t and N_d/N_t were 15.4 per cent and 85 per cent, respectively. The revised SMMSNs of solar cycle 22 reached its largest value in November 1989, and N_a/N_t and N_d/N_t were 46.2 per cent and 53.8 per cent, respectively. N_a/N_t and N_d/N_t for the unrevised SMMSNs in solar cycle 23 were 11.1 per cent and 88.9 per cent, respectively, while N_a/N_t and N_d/N_t for the revised SMMSNs in solar cycle 23 were 50 per cent and 50 per cent, respectively. It is obvious that the solar cycle distributions of strong SPEs under revised SMMSNs is greatly different from that under unrevised SMMSNs for solar cycles 22 and 23. The revised SMMSNs were launched in 2015 July, suggesting that solar cycle distributions of various space weather events by using unrevised SMMSNs (e.g. Le et al. 2012, 2013, 2014) should be re-investigated. The results in

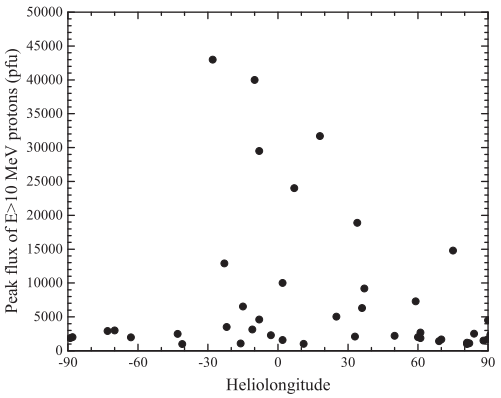

Figure 4. The longitudinal distribution of the strong SPEs with different intensities.

the present study and in the article by Le & Liu (2020) showed that most of the GLE events and strong SPEs, which were produced by the corresponding solar flares and CMEs, appeared around solar maximum. However, seldom of the events with daily flux $\geq 10^{9}$cm^{-2}d^{-1}sr^{-1} for $E > 2$ MeV electrons observed at geostationary orbit, which were mainly caused by the high-speed solar wind came from the coronal hole, occurred around solar maximum (Le, Zhang & Zhao 2021).

(ii) The N-S asymmetry of the strong SPEs is not very clear, as can be seen in Table 1. However, the N-S asymmetry of the strong SPEs is very clear if we calculate the number of the strong SPEs within every 20°, as shown in Table 4. We can see from Table 4 that the range S0–S19 has slightly more strong SPEs than N0–N19. However, N20–N39 has much more strong SPEs than S20–S39. The results indicate that the N-S asymmetry is not obvious in low-middle (0°–19°) latitudes, while the N-S asymmetry is obvious in middle-high ($\geq$20°) latitude area.

(iii) The projected speed of the CME associated with the extreme SPE in solar cycle 23 is $\geq$1443 km s^{-1}, as shown in Table A1 of Appendix A. Noted that the projected speed of the CME associated with the strong SPE on 2005 January 20 was obtained from the article by Gopalswamy et al. (2005). The averaged speeds of the CME-driven shocks accompanied with extreme SPEs during the period from the Sun to the Earth are larger than 1200 km s^{-1}, as shown in Table 3. The source locations and the ITPs of extreme SPEs with peak fluxes $\geq$20 000 pfu indicate that only those CMEs with very high speed and source location around the solar disc centre and the moving direction always toward the Earth can lead to very strong

Table 3. The solar and interplanetary phenomena, and the geoeffectiveness associated with the extreme SPEs.

	Solar activity						Sun–Earth process Time and speed		Geoeffectiveness			ITP
Date yyyy/mm/dd	AR	Location	V_{cme}	FI	Flare time hh:mm	Type-II onset hh:mm	Δt h	$\overline{V}$ km/s	SPE flux pfu	SSC time dd/hhmm	Dst nT	
1989/10/19	5747	S27E10	dg	X13.0	12:55	12:49	20.5	2032.5	40000	20/09:16	−268	P
1991/03/22	6555	S26E28	dg	X9.4	22:23	22:28	29.2	1425.3	43000	24/03:42	−298	P
1994/02/20	7671	N09W02	dg	M4.0	01:41	01:56	31.1	1340.5	10000	21/09:01	−144	P
2000/07/14	9077	N22W07	1674	X5.7	10:24	10:17	28.3	1470.6	24000	15/14:37	−301	P
2000/11/08	9213	N10W75	1738	M7.4	23:28	22:51	31.6	1317.9	14800	10/06:28	−96	O
2001/09/24	9632	S16E23	2402	X2.6	10:38	10:45	33.7	1225.1	12900	25/20:25	−102	P
2001/11/04	9684	N06W18	1810	X1.0	16:20	16:10	33.6	1233.0	31700	06/01:56	−292	P
2001/11/22	9704	S15W34	1437	M9.9	23:30	22:31	31.4	1326.3	18900	24/05:56	−221	P
2003/10/28	10486	S16E08	2459	X17.0	11:10	10:17	19.9	2039.8	29500	29/06:11	−353	P

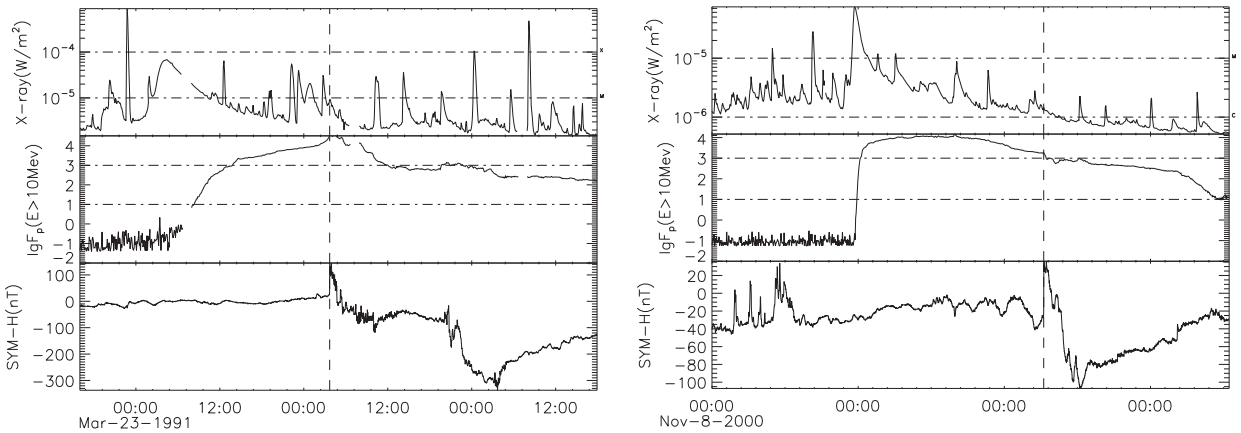

Figure 5. The ITPs for the two SPEs. The left- and right-hand figures are for the SPE that occurred from 1991 March 23 to 24 and for the SPE that occurred 2000 November from 9 to 10. The vertical dashed lines indicate the moment when the shock driven by the associated CME reached the Earth.

Table 4. N-S asymmetry of the strong SPEs for every 20°.

Northern hemisphere		Southern hemisphere	
Latitudinal area	Number of strong SPEs	Latitudinal area	Number of strong SPEs
N0–N19	11	S0–S19	13
N20–N39	12	S20–S39	6
N40–N49	0	S40–S49	1

SPEs with peak fluxes ≥20 000 pfu and super geomagnetic storms (Dst ≤−250 nT), namely that the peak intensity and the ITP of a SPE depend on the source location, speed and direction of propagation of the associated CME. Subsequent CMEs that erupted from the same active region earlier within 24 h or shorter time can also influence the peak fluxes of the associated SPEs (e.g. Kahler 2001; Gopalswamy et al. 2002; Kahler & Vourlidas 2005; Ding et al. 2014). The protons may be accelerated only by the CME-driven shock (Reames 1999) or may be accelerated by both the concurrent flare and CME-driven shock (Kallenrode 2003; Le, Li & Zhang 2017; Le & Zhang 2017; Zhao & Le 2020). The topic of solar and interplanetary sources of solar energetic particles is beyond the scope of the present study.

(iv) The size of solar cycle 25 has been predicted by many researchers (e.g. Jiang & Cao 2018; Jiang et al. 2018; Han & Yin 2019). However, we do not know which one is correct now. The number of strong SPEs that will occur during solar cycle 25 cannot be predicted because of the poor correlation between N_t and SCS.

4 SUMMARY

The main results are summarized as follows:

(i) 43 strong SPEs were recorded in the period between 1976 and 2018. Of the 43 strong SPEs, 27.9 per cent and 20.9 per cent of them were GLE events and extreme SPEs, respectively.

(ii) The statistical results show that 48.8 per cent and 51.2 per cent of the strong SPEs occurred during the rising and declining phases of a solar cycle, respectively. 76.7 per cent of the strong SPEs appeared in the period from two years before to the three years after the solar maximum, indicating that most strong SPEs occurred in this time. The number of strong SPEs in a solar cycle has a poor correlation with the SCS.

(iii) Northern and Southern hemispheres of the Sun have 20 and 23 strong SPEs, respectively. N0–N19 and S0–S19 have 11 and 13 strong SPEs, respectively. There were 12 and 7 strong SPEs in the latitudinal area $N \geq 20°$ and $S \geq 20°$, respectively, indicating that the N-S asymmetry of strong SPEs mainly happened in the latitudinal area above 20° of the two hemispheres.

(iv) The Eastern and Western hemispheres of the Sun have 17 and 26 strong SPEs respectively, indicating that E-W asymmetry is obvious. The strong SPEs were distributed in the region of [E90–W90]. Extreme SPEs appeared within the longitudinal area from E30 to W75, while the SPEs with peak fluxes ≥20 000 pfu concentrated in the range from E30 to W30 and were always accompanied by super geomagnetic storms (Dst ≤−250 nT).

ACKNOWLEDGEMENTS

We thank NOAA for providing the solar soft X-ray, SPE data, the onset time of type-II radio bursts; NASA providing CME catalogue, which is generated and maintained at the CDAW Data Center by NASA and The Catholic University of America in cooperation with the Naval Research Laboratory. SOHO is a project of international cooperation between ESA and NASA; the WDC-SILSO, Royal Observatory of Belgium in Brussels for providing SMMSNs at http://sidc.oma.be/silso/datafiles; and the Center for Geomagnetism and Space Magnetism, Kyoto University, for providing the SYM-H index. We also thank the Institute of Geophysics, China Earthquake Administration for providing SSC data. This work was supported by the National Natural Science Foundation of China (grant nos 41774085, 41074132, 41274193, 41474166, 41774195, and 41874187).

DATA AVAILABILITY

The inclusion of a Data Availability Statement is a requirement for articles published in MNRAS. Data Availability Statements provide a standardized format for readers to understand the availability of data underlying the research results described in the article. The statement may refer to original data generated in the course of the study or to third-party data analysed in the article. The statement should describe and provide means of access, where possible, by linking to the data or providing the required accession numbers for the relevant data bases or DOIs.

REFERENCES

Clette F., Lefèvre L., 2016, Sol. Phys., 291, 2629
Clette F., Svalgaard L., Vaquero J. M., Cliver E. W., 2014, Space Sci. Rev., 186, 35
Clette F., Cliver E. W., Lefèvre L., Svalgaard L., Vaquero J. M., 2015, Space Weather, 13, 529
Clette F., Lefèvre L., Cagnotti M., Cortesi S., Bulling A., 2016, Sol. Phys., 291, 2733
Ding L.-G., Li G., Dong L.-H., Jiang Y., Jian Y., Gu B., 2014, J. Geophys. Res. Space Phys., 119, 1463
Gopalswamy N., Yashiro S., Michałek G., Kaiser M. L., Howard R. A., Reames D. V., Leske R., von Rosenvinge T., 2002, ApJ, 572, L103
Gopalswamy N., Xie H., Yashiro S., Usoskin I., 2005, Proc. 29th Int. Cosmic Ray. Conf., 1, 169
Han Y. B., Yin Z. Q., 2019, Sol. Phys., 294, 107
Iucci N. et al., 2005, Space Weather, 3, S01001
Jiang J., Cao J., 2018, J. Atmos. Sol. Terr. Phys., 176, 34
Jiang J., Wang J.-X., Jiao Q.-R., Cao J.-B., 2018, ApJ, 863, 159
Kahler S. W., 2001, J. Geophys. Res. Space Phys., 106, 20947
Kahler S. W., Vourlidas A., 2005, J. Geophys. Res. Atmos., 110, A12S01
Kallenrode M.-B., 2003, J. Phys. G Nucl. Part. Phys., 29, 965
Le G., Cai Z., Wang H., Zhu Y., 2012, Ap&SS, 339, 151
Le G., Yang X., Ding L., Liu Y., Lu Y., Chen M., 2014, Ap&SS, 352, 403
Le G.-M., Liu G.-A., 2020, Sol. Phys., 295, 35
Le G.-M., Zhang X.-F., 2017, Res. Astron. Astrophys., 17, 123
Le G.-M., Cai Z.-Y., Wang H.-N., Yin Z.-Q., Li P., 2013, Res. Astron. Astrophys., 13, 739
Le G.-M., Li C., Zhang X.-F., 2017, Res. Astron. Astrophys., 17, 73
Le G.-M., Zhang Y.-N., Zhao M.-X., 2021, Sol. Phys., 296, 16
Reames D. V., 1999, Space Sci. Rev., 90, 413
Shea M. A., Smart D. F., 1990, Sol. Phys., 127, 297
Shea M. A., Smart D. F., 1996, Adv. Space Res., 17, 225
Shea M. A., Smart D. F., 2001, Proc. 27th Int. Cosmic Ray. Conf.(Hamburg), p. 3401
Shea M. A., Smart D. F., 2002, Adv. Space Res., 29, 325
Shea M. A., Smart D. F., 2007, Proc. 30th Int. Cosmic Ray. Conf. 261
Shea M. A., Smart D. F., 2012, Space Sci. Rev., 171, 161
Zhang M., Zhao L., 2017, ApJ, 846, 107
Zhao M.-X., Le G.-M., 2020, Res. Astron. Astrophys., 20, 37

APPENDIX A: STRONG SPES DURING 1976–2018

There are 43 in total strong SPEs during solar cycles 21–24, which are listed in Table A1. In the table, columns 1–9 are sequential number, the flare time, the X-ray FI, flare position, the NOAA number of the AR, the time at the SPE peak flux, the peak flux of $E > 10$ MeV protons, CME speed and whether a strong SPE is accompanied by a GLE, respectively. To be noticed that we have no CME information for the SPEs that occurred during solar cycles 21 and 22.

Table A1. The strong SPEs during 1976–2018.

No	Flare				SPE		V_{CME}	GLE?
	Time yyyy/mm/dd/hhmm	X-ray peak	Location	Active region	Time yyyy/mm/dd/hhmm	> 10 MeV peak flux pfu	km s^{-1}	
1	1978/04/28/1306	X5	N22E41	1092	1978/04/30/2000	1000		No
2	1978/09/23/1023	X1	N35W50	1294	1978/09/24/0400	2200		Yes
3	1981/10/07/2308	X3	S19E88	3390	1981/10/13/247	2000		No
4	1982/07/09/0742	X9	N17E73	3804	1982/07/13/1615	2900		No
5	1982/12/07/2354	X2	S14W81	4007	1982/12/08/1000	1000		Yes
6	1984/04/25/0005	X13	S12E43	4474	1984/04/26/1420	2500		No
7	1989/03/10/1405	X4.5	N31E22	5395	1989/03/13/0645	3500		No
8	1989/03/17/1737	X6.5	N33W60	5395	1989/03/18/0920	2000		No
9	1989/08/12/1427	X2.6	S16W37	5629	1989/08/13/0710	9200		No
10	1989/09/29/1133	X9.8	S26W90	5698	1989/09/30/0210	4500		Yes
11	1989/10/19/1258	X13.0	S27E10	5747	1989/10/20/1600	40000		Yes
12	1989/11/30/1225	X2.6	N26W59	5800	1989/12/01/1340	7300		No
13	1991/03/22/2245	X9.4	S26E28	6555	1991/03/24/0350	43000		No
14	1991/06/04/0352	X12.0	N30E70	6659	1991/06/11/1420	3000		No
15	1991/06/15/0821	X12.0	N33W69	6659	1991/06/15/1950	1400		Yes
16	1991/07/07/0223	X1.9	N26E03	6703	1991/07/08/1645	2300		No
17	1992/05/08/1546	M7.4	S26E08	7154	1992/05/09/2100	4600		No
18	1992/10/30/1816	X1.7	S22W61	7321	1992/10/31/0710	2700		No
19	1994/02/20/0141	M4.0	N09W02	7671	1994/02/21/0900	10000		No
20	1998/04/20/1021	M1.4	S43W90	8194	1998/04/21/1205	1700	1863	No
21	1998/09/30/1350	M2.8	N23W81	8340	1998/10/01/0025	1200	DG[a]	No
22	2000/07/14/1024	X5.7	N22W07	9077	2000/07/15/1230	24000	1674	Yes
23	2000/11/08/2328	M7.4	N10W75	9213	2000/11/09/1555	14800	1738	No
24	2001/04/02/2151	X20.0	N18W82	9393	2001/04/03/0745	1110	2505	No
25	2001/09/24/1038	X2.6	S16E23	9632	2001/09/25/2235	12900	2401	No
26	2001/10/01/0515	M9.1	S22W91	9628	2001/10/02/0810	2360	1405	No
27	2001/11/04/1620	X1.0	N06W18	9684	2001/11/06/0215	31700	1810	Yes
28	2001/11/22/2330	M9.9	S15W34	9704	2001/11/24/0555	18900	1443	No
29	2002/04/21/0151	X1.5	S14W84	9906	2002/04/21/2320	2520	2393	No
30	2003/10/28/1110	X17.0	S16E08	10486	2003/10/29/0615	29500	2459	Yes
31	2003/10/29/2049	X10.0	S15W02	10486	2003/11/03/0815	1570	2029	Yes
32	2004/07/25/1514	M1.1	N08W33	10652	2004/07/26/2250	2086	1333	No
33	2005/01/17/0952	X3.8	N15W25	10720	2005/01/17/1750	5040	2547	Yes
34	2005/01/20/0701	X7.1	N14W61	10720	2005/01/20/0810	1860	3242	Yes
35	2005/05/13/1657	M8.0	N21E11	10759	2005/05/15/0240	3140	1689	No
36	2005/09/07/1740	X17.0	S06E89	10808	2005/09/11/0425	1880	ND[b]	No
37	2006/12/06/1847	X6.5	S06E63	10930	2006/12/07/1930	1980	ND	No
38	2012/01/23/0359	M8.7	N28W36	11402	2012/01/24/1530	6310	2175	No
39	2012/03/07/0024	X5.4	N17E15	11429	2012/03/08/1115	6530	2684	No
40	2013/05/22/1332	M5.0	N15W70	11745	2013/05/23/0650	1660	1460	No
41	2014/01/07/1832	X1.2	S15W11	11944	2014/01/09/0340	1026	1830	No
42	2015/06/21/0236	M2.6	N12E16	12371	2015/06/22/1900	1070	1366	No
43	2017/09/10/1606	X8.2	S08W88	12673	2017/09/11/1140	1490	3163	Yes

Notes: [a] DG: data gap LASCO out of work.
[b] ND: no data LASCO worked normally.

This paper has been typeset from a TEX/LATEX file prepared by the author.